Ionizing Radiation induces cells with past caspase activity that contribute to the adult organ in *Drosophila* and show reduced Loss of Heterozygosity

Sarah Colon Plaza and Tin Tin Su[1]
Department of Molecular, Cellular and Developmental Biology, University of Colorado at Boulder, CO, 80309-0347

[1]Corresponding author; tin.su@colorado.edu

Abstract
There is increasing recognition that cells may activate apoptotic caspases but not die, instead displaying various physiologically relevant consequences. We know very little, however, of the mechanisms that underlie the life/death decision in a cell that has activated apoptotic caspases. By optimizing a published reporter for past caspase activity, we were able to visualize cells that survived caspase activation specifically after exposure to ionizing radiation in *Drosophila* larval wing discs. We found that cells with X-ray-induced past active caspases (XPAC) do not arise at random but are born at specific locations within the developing wing imaginal discs of *Drosophila* larvae. We found also that the apoptotic signaling pathway is needed to induce XPAC cells. Yet, XPAC cells appear in stereotypical patterns that do not follow the pattern of IR-induced apoptosis, suggesting additional controls at play. Functional testing identified the contribution of *wingless* (*Drosophila* Wnt1) and Ras signaling to the prevalence of XPAC cells. By following irradiated larvae into adulthood, we found that XPAC cells contribute to the adult wing. To address the relationship between XPAC and genome stability, we combined a reporter for past caspase activity with *mwh*, an adult marker for Loss of Heterozygosity (LOH). We found a lower incidence of LOH among XPAC compared to cells that did not activate the reporter for past caspase activity. In addition, at time points when wing disc cells are finishing DNA repair, XPAC cells show an anti-correlation with cells with unrepaired IR-induced double-stranded breaks. Our data suggest that non-lethal caspase activity safeguards the genome by facilitating DNA repair and reducing LOH after transient exposure to X-rays. These results identify a physiological role for non-lethal caspase activity during recovery from radiation damage.

Key words: ionizing radiation, X-rays, *Drosophila*, apoptosis, Wnt, Ras, caspase, loss of heterozygosity

Conflict of Interest: Authors declare no competing financial interests in relation to the work described.

36 **Introduction**
37 An exciting emerging field is based on the recognition that cells may activate apoptotic caspases but not
38 die, instead displaying various physiologically relevant consequence such as axon pruning and reduction
39 of the cytoplasm during sperm maturation (for reviews, (1-4)). In one variation, a cell may return to life
40 from the brink of apoptotic death in a process called anastasis (2, 5-7), which is seen in cultured cells
41 exposed to a variety of death stimuli including ethanol (8), a broad-spectrum kinase inhibitor
42 Staurosporine and a small molecule BCL-2 antagonist (9), or ion beam radiation (10). Removal of death-
43 inducing stimuli before apoptosis is completed allows some cells to recover even after displaying such
44 apoptotic features as cleaved caspases, Mitochondrial Outer Membrane Permeabilization, or
45 phosphatidylserine flipping. Cells that underwent anastasis are not only alive but are capable of
46 proliferation and initiating tumors. How cells activate apoptotic caspases but not die is still poorly
47 understood. Dissecting this phenomenon requires the ability to detect cells that activated caspases but
48 did not die. Two genetic reporters for past caspase activity have been described in *Drosophila*
49 *melanogaster* (11, 12). CasExpress and Caspase Tracker relies on the transcriptional activator GAL4 with
50 a cell-membrane tether that includes a recognition sequence, DQVD, for effector caspase Drice
51 (*Drosophila* caspase 3/7 in conjunction with the G-trace lineage tracing system (13)). Upon Drice
52 activation, the tether is cleaved and GAL4 enters the nucleus to initiate the expression UAS-FLP
53 recombinase, which catalyzes a recombination event to cause permanent GFP expression. Both sensors
54 show widespread non-lethal caspase activity in nearly every tissue during *Drosophila* development (11,
55 12). CasExpress reporter was used in a screen for regulators of developmental non-lethal caspase
56 activity that identified apical caspase Dronc, caspase inhibitor p35, pro-survival signaling component
57 Akt, transcription factor dCIZ1 and Ras (14). One of these, dCIZ1, was shown to promote survival after
58 caspase activation by heat shock, oncogenic stress and X-rays.
59
60 We wanted study cells with past caspase activity induced not by developmental events but by ionizing
61 radiation (IR). IR is used to treat more than half of cancer patients where therapeutic success relies on
62 IR's ability to induce apoptosis. Therapy failure can result if cells initiate but do not complete apoptosis
63 after IR exposure, making it important to understand molecular mechanisms that regulate the
64 production of such cells. The use of CasExpress and Caspase Tracker to detect IR-induced non-lethal
65 caspase activation have been challenging because of strong developmental signals from these
66 biosensors even when GAL4 activity is temporally controlled with the temperature sensitive repressor
67 $GAL80^{ts}$ (15). Here, we report an optimized temperature shift protocol that out-performs published
68 protocols by increasing the ratio of IR-induced to constitutive signal from ~2-4 to ~20. This allows us to
69 detect cells with past caspase activity that results specifically from exposure to X-ray, a type of IR. We
70 found that cells with X-ray-induced past active caspases (XPAC) do not arise at random but are born at
71 specific locations within the developing wing imaginal discs of *Drosophila* larvae. Inhibition of apoptotic
72 signaling reduced the prevalence of XPAC cells. Yet, XPAC cells appear in stereotypical patterns that do
73 not follow the pattern of IR-induced apoptosis, suggesting additional controls at play. Functional testing
74 identified Wg (Wnt1) pathway and Ras signaling as such controls. By following irradiated larvae into
75 adulthood, we found that XPAC cells contribute to the adult wing. Anastasis has been associated with
76 increased genome instability in immortalized mammalian cells (7, 9, 10). On the other hand, wide-
77 spread non-lethal caspase activity is detected during normal *Drosophila* development, raising the
78 possibility that such activity may be neutral or even beneficial to healthy cells. XPAC cells, we found,
79 show reduced Loss of Heterozygosity (LOH), suggesting that non-lethal caspase activity safeguards the
80 genome after transient exposure to X-rays in *Drosophila*.
81

Results

Optimizing temperature shift conditions to detect cells with past ionizing radiation-induced caspase activity

In our published work with Caspase Tracker, we raised the larvae at 18°C and shifted them to 29°C to inactivate GAL80^{ts} from 0 to 6h after exposure to 4000R (40Gy) of X-rays (15) (Fig. 1A, T=29°C). 4000R is typically used in *Drosophila* because it kills more than half of the cells in a wing disc but is still compatible with regeneration and survival as viable fertile adults can emerge. We chose a 6h temperature shift based on the literature. *hid* and *rpr,* which encode SMAC orthologs and are essential for IR-induced caspase activation, are transcriptionally induced at 2h after IR (16). Caspase cleavage and staining with the vital dye Acridine Orange (AO) are detectable at 3h after IR; AO stains apoptotic and not necrotic cells in *Drosophila* (17). By 4h after IR, *hid/rpr* expression has declined compared to the 2h time point, although cleaved caspases and AO staining remain visible for up to 24h after (16). Based on these results, a 6h window immediately after IR would capture the bulk of IR-induced caspase activation.

Even with limited (6h) activation of GAL4, unirradiated wing discs from unirradiated larvae show GFP+ cells (Fig. 1C', quantified in Fig. 1B, 29° -IR datasets), as we reported before [20] . Although the GFP+ area increased significantly with irradiation by 3-fold for Caspase Tracker and 4-fold for CasExpress (Fig. 1D', quantified in B), high constitutive signal means about 66% of Caspase Tracker>GFP cells and about 75% of CasExpress>GFP cells in irradiated discs are X-ray-induced while the remainder are from developmental caspase activation. To eliminate the GFP signal from the latter, we tried using lower temperatures to inactivate GAL80 in the protocol in Fig. 1A (Figure 1 E-G'), using CasExpress that shows smaller variance than Caspase Tracker -IR (Fig. 1B). We found that we could go as high as 26°C and still keep the CasExpress>GFP area to near zero in unirradiated discs (Fig. 1G', quantified in B) while IR increased the GFP+ area significantly (Fig. 1H', quantified in B). A control CasExpress sensor with a DQVD->DQVA mutation showed no GFP+ cells even with IR (compare Fig. 1I to H'), indicating that GFP+ cells report effector caspase activity specifically. Returning the larvae back to 18°C immediately after irradiation, that is, without any temperature shift, eliminated GFP+ cells (Fig. 1J), indicating that production of GFP+ cells is GAL4-dependent. Because of low GFP+ area without IR at 26°C, the 'signal to noise' ratio increased to 20-fold, meaning most (>90%) of GFP+ cells +IR discs were cells with X-ray-induced past active caspases (XPAC). Subsequent experiments use the protocol in Fig. 1A with T=26°C.

XPAC *cells proliferate*

The data in Fig. 1 were from 3 days after irradiation. To study GFP+ XPAC cells soon after they form, we performed a time course (Fig. 2). GFP+ cells were not observed at 6h after IR but were readily detectable at 24h after IR (Fig. 2A). At this timepoint, most GFP+ cells were either singlets or in small groups of 2-5 cells. These results agree with the published timings of check point arrest, recovery and cell doubling in the wing disc. 4000R of X-rays stops the cell cycle via checkpoint activation, with S phase and mitosis resuming at about 6h after irradiation (18). Cell doubling times in 3rd instar wing discs average 12h (19). Therefore, at 24h after irradiation, cells would have divided on average just once, which can be seen as the appearance of singlets (arrow) and doublets (arrowhead) in Fig. 2A. At 48h after irradiation, single GPF+ cells were rare and most cells were in clones of 4-30 cells each (Fig. 2B). Clone size increased further at 72h after IR, the last time point taken before we lost the larvae to pupariation (Fig. 2C). We conclude that XPAC cells are capable of clonogenic proliferation. Real time marker RFP was not observed presumably because the return to 18°C restored GAL80^{ts} and repressed GAL4.

The prevalence and the location of XPAC cells change with development

129 Our collection of larvae spanned 24h in age and show a range of developmental stages, that is, wing
130 discs of different sizes and degree of epithelial folding (Figure 3A-D, arrowheads). We noticed three
131 trends in the prevalence and the location of GFP+ XPAC cells at 24h after IR. First, smaller discs showed
132 more GFP+ area relative to the disc size than larger, more developed discs (compare Fig. 3D' to A'). A
133 plot of % disc area, that is GFP+ against disc size illustrates this trend (Fig. 3F '6-7d at IR'). The area
134 serves as surrogate for cell number since wing discs are composed of a single layer epithelium. We
135 quantified clone area instead of clone number to avoid errors in assigning cells to clones, especially as
136 XPAC cells appear close together (Fig 2A-C). By using an early (24h) time point, we are catching XPAC
137 cells soon after birth and before cell division makes a significant contribution to clone area (see
138 preceding paragraph). We interpret the dependence of XPAC prevalence on disc size to mean that as the
139 disc increased in developmental age, X-rays were able to induce fewer cells that activated caspases but
140 survived. This correlation was confirmed by aging the larvae for an additional 24h at 18°C before
141 irradiation. This produced larger, more developed discs. Importantly, the same relationship between
142 disc size and % GFP+ area was seen in the older cohort (Fig. 3F, '7-8d at IR'), except that overall values
143 shifted to the right as expected for older discs. Separating discs based on the absence or presence of
144 epithelial folds, a criterion used before to separate discs according to development (20), led to the same
145 conclusion; more developed discs had fewer XPAC cells (Fig. 3G).
146
147 Second, the distribution of GFP+ cells in each disc was not homogenous. The notum (future body wall or
148 'n' in Fig. 3A') had fewer GFP+ cells than the future wing ('w' in Fig. 3A' includes the hinge and the
149 pouch). This was true regardless of disc size. Third, when the number of GFP+ cells declined in larger
150 discs, their loss began in the distal pouch (* in Fig. 3A', B', C'), leaving a ring of GFP+ cells (Fig. 3C',
151 arrows).
152
153 ***Apoptosis signaling can increase or decrease XPAC prevalence***
154 We next investigated the role of apoptotic signaling in XPAC cells. Using UAS-transgenes, we increased
155 apoptotic signaling with *hid* and *rpr* together or *rpr* alone and decreased apoptotic signaling with a
156 dominant negative version of apical/initiator caspase Dronc (apical caspase) or p35 (effector caspase
157 inhibitor). This means only in cells that have initiated caspase activation and translocated GAL4 into the
158 nucleus as part of the CasExpress system would express the transgenes cell-autonomously, identifying
159 what keeps cells alive <u>after</u> they began to activate apoptotic caspases. We used also heterozygotes for
160 the H99 chromosomal deficiency that removes *hid*, *rpr* and *grim* and has been shown to reduce and
161 delay IR-induced apoptosis (16); the effect of H99 would be throughout the organism and not just cell-
162 autonomous or conditional. We analyzed discs with no folds because their robust XPAC incidence
163 (~30%) provides room to detect changes up or down. Both, increasing and decreasing apoptotic
164 signaling reduced XPAC prevalence (Fig 3H). The seemingly paradoxical result can be explained by the
165 threshold model wherein active caspases cleave and activate other caspases (21, 22), thus amplifying
166 caspase activity to reach a certain level needed for cell death (23). We propose a second, lower
167 threshold for successful recombination and permanent GFP expression (Fig 3I). Here, initial Drice activity
168 translocates GAL4 into the nucleus but $Dronc^{DN}$ and p35 become expressed to prevent the amplification
169 needed to reach the threshold for successful recombination and permanent GFP expression. H99 would
170 reduce effector caspase activity, preventing some cells from activating CasExpress, thus also reducing
171 the number of GFP+ cells. At the other end of the continuum, increasing effector caspase activity with
172 *hid*/*rpr* would push cells over the threshold for cell death, reducing the number of GFP+ cells that
173 activated apoptotic caspases but lived. In sum, we propose that decreasing or increasing apoptotic
174 signaling will keep a cell out of the intermediate zone of caspase activity needed to produce a GFP+ cell.
175
176 ***Developmental changes in XPAC induction does not correlate with apoptosis or cell proliferation***

177 We next addressed why the prevalence of GFP+ cells decline in more developed discs. One possibility is
178 cell cycle exit; non-dividing cells are known to be refractory to apoptosis, for example in *Drosophila* eye
179 disc (24). Unlike in the eye disc, however, cells in the wing disc continue to proliferate throughout larval
180 stages except for 4-cell wide Zone of Non-proliferating Cells (ZNC) along the dorsoventral boundary in
181 the late 3rd instar wing disc that arrest in G1/G2 (25). Cell cycle exit is unlikely to explain the reduction in
182 XPAC prevalence with developmental stage for the two reasons. First, at 24h after IR when cells have
183 already recovered from checkpoint arrest (18), antibody staining for phospho-Histone H3, a mitotic
184 marker, showed robust and wide-spread mitoses including in most developed discs in our samples
185 where we see no XPAC cells (Fig 4C-C''). Specifically, we noted robust mitotic activity in the notum
186 (arrows) and the pouch (between dashed lines) that includes the future ZNC. Second, the notum and the
187 pouch have similar cell doubling times (20), yet, as the wing disc develops, XPAC cells are lost from the
188 notum before they are lost from the pouch (Fig 4B''). We conclude that cell cycle exit is unlikely to be
189 the cause for XPAC reduction that accompanies development.
190
191 The possibility is that X-rays were less efficient at inducing caspase activity in more developed discs is
192 also unlikely. Cleaved active Dcp1 is absent without irradiation (S1 Figure) but is readily discernable in
193 irradiated discs regardless of whether they show robust XPAC induction (Fig 4D'' and E'') or only a few
194 detectable GFP+ cells (Fig 4F''). The notum (arrow) and the distal pouch (*) in particular show robust
195 Dcp1 signal yet display reduced XPAC prevalence as the discs mature. AO staining 4 h after IR confirmed
196 that the induction of wide-spread cell death at developmental stages we study (Fig 4G-H; the brackets
197 indicate the hinge cells that we showed before are refractory to IR-induced apoptosis (24)). We
198 conclude that while apoptotic caspase activity is necessary to generate XPAC cells (Fig 3), it is not
199 sufficient to explain the spatiotemporal distribution of XPAC cells, which does not match the
200 spatiotemporal distribution of IR-induced caspase activation. We infer that other mechanisms operate
201 on top of caspase activation to decide whether a cell with active caspases live or die.
202
203 ***Wg and Ras Signaling modulate XPAC prevalence***
204 The changing pattern of XPAC cells as discs develop suggests that developmental signaling pathways
205 may play a role. We focused on Wg (Wnt1) and Ras because they are (1) active in the regions of the wing
206 disc with dynamic XPAC prevalence and (2) are known to influence cell survival. For example, XPAC cells
207 clear from the distal pouch around a line of Wg-expressing cells (yellow arrowhead in Fig 5C) while they
208 persist near the Wg Inner Ring (white arrowhead in Fig 5C). As for apoptotic signaling in Fig 3, we used
209 UAS-transgenes to express Wg, Axin (Wg inhibitor) or RAS^{G12V} (constitutively active RAS) specifically in
210 CasEx-GAL4-active cells for 6h after IR. All three transgenes significantly lowered the XPAC prevalence
211 (Fig 5E-F), which is reminiscent of how both increased and decreased apoptotic signaling lowered XPAC
212 prevalence (Fig 3H). Lower XPAC prevalence we see after inhibition of Wg is unlikely to be indirect via
213 delayed development because less developed discs show more XPAC. Given the known anti-apoptotic
214 role of Wg (24), the model in Fig 3I could explain the Wg/Axin results. Specifically, inhibiting Wg with
215 Axin could drive cells over the threshold for cell death while increased Wg could keep the cell below the
216 threshold for CasEx>GFP. Staining for cleaved active Dcp1 supports this idea (Fig 5G); Wg inhibited while
217 Axin promoted caspase activation. The threshold model can also explain the results with RAS^{G12V} (Fig 5F).
218 Ras/MAPK signaling is known to inhibit caspase activation, by direct phosphorylation and inhibition of
219 Hid during *Drosophila* eye development, for example (26). Inhibition of Drice activity by RAS^{G12V} could
220 keep the cell below the threshold for CasEx>GFP, lowering XPAC prevalence. RAS^{G12V} reduced cleaved
221 Dcp1 signal, supporting this idea.
222
223 ***Cells with past caspase activity show reduced IR-induced LOH***

We next addressed the consequences of past IR-induced caspase. Cultured human cells exposed to 0.5 Gy (50R) of particle radiation, a type of IR, show persistent caspase activation for up to two weeks without dying, elevated DNA breaks and oncogenic transformation (10). X-rays on the other hand induce transient caspase activation, with DNA breaks clearing within 24h post IR exposure in larval wing discs (18, 24). To assay for long term effects of non-lethal caspase activity under these conditions, we followed XPAC cells into adult wings where they appear in an IR-dependent manner (Fig. 6) regardless of larval age at the time of irradiation (6-7d or 7-8d; corresponding to larval XPAC data in Fig. 3F). This allows us to use the *multiple wing hair* adult marker to quantify Loss of Heterozygosity (LOH), a type of genome aberration. LOH of recessive *mwh* alleles results in homozygous mutant cells with more than one hair each due to defective actin organization (27). We showed previously that *mwh* LOH is absent without IR but is induced when larvae are irradiated with 4000R of X-rays (28). At appropriate magnification, it is possible to assign GFP and *mwh* status to each cell (Fig. 6H). We found that *mwh* incidence was lower for GFP+ relative to GFP- areas of the same wing (Fig. 6I).

There are two possible interpretations of the data that cells with XPAC show reduced LOH. Non-lethal caspase activity may facilitate DNA repair to reduce genome instability or non-lethal caspase activity and chromosome breaks may act in a synthetic lethal combination to take the cell above the threshold for apoptosis, thereby eliminating such cells. To distinguish between these possibilities, we monitored DNA repair kinetics after irradiation and correlated them with non-lethal caspase activity. γ-H2Av signal (fly γ-H2Ax) is detected in all cells of the wing disc after exposure to 4000R of X-rays indicative of DNA double strand breaks induction (4h timepoint shown in S1 Figure) but returns to background levels 24h after IR as repair is completed (18, 24). Consistent with these data, at 20-22h after IR, only a subset of cells show γ-H2Av staining (Fig 6 J-L’’’’), which we interpret as cells that have yet to complete DNA repair. CasEx>GFP, which becomes detectable at similar times, show mutual exclusion with γ-H2Ax; cells that show both are rare (arrowheads in Fig 6J’’’’). We interpret these results to mean that XPAC cells complete DNA repair more efficiently than their GFP-counterparts. More efficient repair in XPAC cells, we propose, could explain the observed reduction in LOH in the adult wing.

Discussion

We report here a study of cells with X-ray induced past active caspases (XPAC) during wing development in *Drosophila*. An optimized temperature shift protocol allowed us to minimize cells with spontaneous, developmental caspase activity and to focus specifically on XPAC cells. Such cells, we found, were able to proliferate and contribute to the adult organ and show reduced genome aberrations as measured by LOH, which results primarily from aneuploidy of whole or segments of chromosomes in *Drosophila* (29). In mouse embryo fibroblasts and immortalized human epithelial cells and fibroblasts (MCF10A and IMR90) exposed to ^{56}F ion particle radiation, caspase activity, γ-H2Ax signal and DNA fragmentation persisted for weeks (10). Irradiated MCF10A cells with high caspase reporter activity formed colonies in soft agar compared to irradiated cells with low reporter activity. Inhibition of caspase 3 using shRNA or a dominant negative construct reduced the colony number, suggesting that caspase activity was causing transformation. While contrary to the findings in mammalian cells, our LOH results are consistent with the wide-spread non-lethal caspase activity during development in *Drosophila* (11, 12) and other metazoans. Clearly, caspases activity in these cases is not causing DNA fragmentation or it would have been detected in multiple studies that monitored DNA breaks (e.g., (18, 24)). We interpret our data to mean that non-lethal caspase activity protects the genome from X-ray-induced chromosome breaks. Unlike with ^{56}F radiation, X-ray-induced DSBs are cleared within 24h, even with much higher IR doses of 4000R (40 Gy) (18, 24). DNA repair may be more efficient in wing disc cells and that in this context, non-lethal caspase activity is beneficial. The question is, how? Caspase-driven cellular transformation in the above cited studies was proposed to occur because caspases work through endonuclease G to unravel

272 the genome to allow access to oncogenic transcription factors such as KRAS/E1A used in these studies
273 (10). Likewise, caspases could make the genome more accessible to DNA repair enzymes instead of
274 transformation factors in the wing disc. In other words, consequences of non-lethal caspase activity may
275 depend on the cellular context, specifically, which proteins are present and active to access the DNA. In
276 cells predisposed to transformation such as immortalized cell lines, the outcome may be transformation.
277 In cells that lack transformation factor but are robustly expressing DNA repair enzymes, improved repair
278 may be the outcome.
279
280 A prior study used the CasEx>GFP reporter and found that Dronc and p35 affect developmental non-
281 lethal caspase activity (14), similar to what we see for XPAC, and identified Akt and transcription factor
282 dCIZ1 as new regulators of developmental CasEx>GFP induction. One striking difference, however,
283 concerns the effect of oncogenic Ras. It preserves cells with developmental caspase activation;
284 expression of Ras^{V12} in the posterior compartment of wing discs increased CasEx>GFP area by 2-fold. In
285 contrast, Ras^{V12} decreased the XPAC area by 2-fold (Fig 5F), which we attribute to its ability to prevent
286 caspase amplification like Wg, $Dronc^{DN}$ and p35 (Fig. 3H). We conclude that retention of cells with past
287 caspase activity shows common as well as different regulatory controls depending on whether cells are
288 subject to developmental or IR-induced caspase activity.
289
290 **MATERIALS AND METHODS**
291 ***Drosophila* stocks**
292 *Drosophila* stocks are listed in S1 Table and include Caspase Tracker (12), UAS-hid/rpr (30), UAS-Wg (31)
293 and UAS-$Dronc^{DN}$ (32). The following stocks were generated using standard *Drosophila* techniques:
294 Caspase Tracker/CyO-GFP; $GAL80^{ts}$/$GAL80^{ts}$
295 Caspase Tracker/CyO-GFP; mwh^{1}/TM6 Tb
296 G-trace/CyO-GFP; UAS-X/TM6 Tb where X was UAS-Wg, UAS-Axin, UAS-p35, UAS-$Dronc^{DN}$, UAS-
297 Ras^{V12}, UAS-$Notch^{ICD}$, UAS-mam^{Δ}, or H99
298 G-trace/CyO-GFP; $GAL80^{ts}$/$GAL80^{ts}$
299 UAS-hid, UAS-rpr/UAS-hid, UAS-rpr or Y; G-trace/CyO-GFP
300 UAS-rpr/UAS-rpr or Y; G-trace/CyO-GFP
301
302 **Larvae culture, temperature shift and irradiation**
303 After crossing virgins and males, the adults were fed on Nutri-Fly German Formula food (Genesee
304 Scientific) for 3 days at 25°C to boost egg production, before transferring them to 18°. Embryos were
305 collected and larvae were raised on Nutri-Fly Bloomington Formula food (Genesee Scientific). The
306 cultures were monitored daily for 'dimples' on the food surface that denotes crowding and split as
307 needed. Larvae in food were placed in petri dishes and irradiated at room temperature (rt) in a Faxitron
308 Cabinet X-ray System Model RX-650 (Lincolnshire, IL) at 115 kV and 5.33 rad/sec. Irradiated larvae in
309 food were placed in new vials in temperature bath filled with Lab Armor beads (ThermoFisher), which
310 we found gave more consistent and reproducible data than water baths. After the temperature shift to
311 inactivate GAL80, larvae were returned to 18°C until dissection.
312
313 **Tissue preparation, staining and imaging**
314 For Acridine Orange staining, Larvae were dissected in PBS, and imaginal discs were incubated for 5 min
315 in PBS+0.5 mM AO (Sigma) at rt, washed twice with PBS, mounted in PBS, and imaged immediately. For
316 γ-H2Av staining, wing discs were dissected in PBS, fixed in 2% paraformaldehyde (PFA) in PBS for 45 min,
317 washed twice with PBS and permeabilized in PBS+0.5% Triton X-100 for 12.5 min. For other antibodies,
318 wing discs were dissected in PBS, fixed in 4% PFA in PBS for 30 minutes, washed thrice in PBS,
319 permeabilized in PBS+0.5% Triton X-100 for 10 min, and rinsed in PBTx (0.1% Triton X-100). The discs

were blocked in 5% Normal Goal Serum in PBTx for at least 1 h and incubated overnight at 4°C in primary antibody in block. Primary antibodies were to cleaved Dcp1 (1:100, rabbit polyclonal, Cell Signaling Cat# 9578), Phospho-Histone H3 (1:1000, rabbit monoclonal, Upstate Biotech), Wg (1:100, mouse monoclonal, DSHB#4D4) and γ-H2Av (1:1000, mouse monoclonal, DSHB#UNC93-5.2.1). The discs were rinsed thrice in PBTx and blocked for at least 30 min before incubation in secondary antibody in block for 2 h at room temperature. Secondary antibodies were used at 1:400-500 (Jackson). The discs were washed in PBTx and stained with 10 ug/ml Hoechst33258 in PBTx for 2 min, washed 3 times, and mounted on glass slides in Fluoromount G (SouthernBiotech).

For adult wings, newly eclosed adults with unfurl wings were collected and kept at rt. The wings were collected within 30 min of unfurling, submerged in PBTx, mounted in Fluoromount G (SouthernBiotech), and imaged immediately. Any delay meant the loss of fluorescence as wing epithelial cells are eliminated in a developmentally regulated wing maturation step [28, 29].

Wing discs and wings were imaged on a Leica DMR compound microscope using a Q-Imaging R6 CCD camera and Ocular or Micro-Manager software. Images were processed and analyzed using ImageJ software.

Statistical Analysis

For sample size justifications, we used a simplified resource equation from (33); E = Total number of animals − Total number of groups, where E value of 10-20 is considered adequate. When we compare two groups (e.g., -/+IR), n= 6 per group or E = 11 would be adequate. All samples exceed this criterion. 2-tailed Student t-test with equal variance was used.

Acknowledgements (include funding sources)

Drosophila stocks from the Bloomington *Drosophila* Stock Center (NIH P40 OD018537) were used in this study. The authors thank Hardwick and Tang labs for Caspase Tracker stocks, Montell lab for CasExpress stocks, and Kristin White for the critical reading of the manuscript. This work was funded by an NIH grant and a diversity supplement to TTS (R35 GM130374) and an NIH fellowship to SCP (F31 GM149184). Monoclonal antibodies developed by Joshua Sanes, Stephen Cohen, and R. Scott Hawley were obtained from the Developmental Studies Hybridoma Bank, created by the NICHD of the NIH and maintained at The University of Iowa, Department of Biology, Iowa City, IA 52242.

350 **References**

351 1. Chakraborty S, Mir KB, Seligson ND, Nayak D, Kumar R, Goswami A. Integration of EMT and
352 cellular survival instincts in reprogramming of programmed cell death to anastasis. Cancer Metastasis
353 Rev. 2020;39(2):553-66.
354 2. Gudipaty SA, Conner CM, Rosenblatt J, Montell DJ. Unconventional Ways to Live and Die: Cell
355 Death and Survival in Development, Homeostasis, and Disease. Annu Rev Cell Dev Biol. 2018;34:311-32.
356 3. Su TT. Non-apoptotic roles of apoptotic proteases: new tricks for an old dog. Open Biol.
357 2020;10(8):200130.
358 4. Tang HM, Tang HL. Anastasis: recovery from the brink of cell death. R Soc Open Sci.
359 2018;5(9):180442.
360 5. McArthur K, Kile BT. Apoptotic Caspases: Multiple or Mistaken Identities? Trends Cell Biol.
361 2018;28(6):475-93.
362 6. Nakajima YI, Kuranaga E. Caspase-dependent non-apoptotic processes in development. Cell
363 Death Differ. 2017;24(8):1422-30.
364 7. Tang HL, Tang HM, Mak KH, Hu S, Wang SS, Wong KM, et al. Cell survival, DNA damage, and
365 oncogenic transformation after a transient and reversible apoptotic response. Mol Biol Cell.
366 2012;23(12):2240-52.
367 8. Tang HM, Talbot CC, Jr., Fung MC, Tang HL. Molecular signature of anastasis for reversal of
368 apoptosis. F1000Res. 2017;6:43.
369 9. Ichim G, Lopez J, Ahmed SU, Muthalagu N, Giampazolias E, Delgado ME, et al. Limited
370 mitochondrial permeabilization causes DNA damage and genomic instability in the absence of cell death.
371 Mol Cell. 2015;57(5):860-72.
372 10. Liu X, He Y, Li F, Huang Q, Kato TA, Hall RP, et al. Caspase-3 promotes genetic instability and
373 carcinogenesis. Mol Cell. 2015;58(2):284-96.
374 11. Ding AX, Sun G, Argaw YG, Wong JO, Easwaran S, Montell DJ. CasExpress reveals widespread and
375 diverse patterns of cell survival of caspase-3 activation during development in vivo. Elife. 2016;5.
376 12. Tang HL, Tang HM, Fung MC, Hardwick JM. In vivo CaspaseTracker biosensor system for
377 detecting anastasis and non-apoptotic caspase activity. Sci Rep. 2015;5:9015.
378 13. Evans CJ, Olson JM, Ngo KT, Kim E, Lee NE, Kuoy E, et al. G-TRACE: rapid Gal4-based cell lineage
379 analysis in Drosophila. Nat Methods. 2009;6(8):603-5.
380 14. Sun G, Ding XA, Argaw Y, Guo X, Montell DJ. Akt1 and dCIZ1 promote cell survival from apoptotic
381 caspase activation during regeneration and oncogenic overgrowth. Nat Commun. 2020;11(1):5726.
382 15. Verghese S, Su TT. Ionizing radiation induces stem cell-like properties in a caspase-dependent
383 manner in Drosophila. PLoS Genet. 2018;14(11):e1007659.
384 16. Wichmann A, Jaklevic B, Su TT. Ionizing radiation induces caspase-dependent but Chk2- and p53-
385 independent cell death in Drosophila melanogaster. Proc Natl Acad Sci U S A. 2006;103(26):9952-7.
386 17. Abrams JM, White K, Fessler LI, Steller H. Programmed cell death during Drosophila
387 embryogenesis. Development. 1993;117(1):29-43.
388 18. Wells BS, Johnston LA. Maintenance of imaginal disc plasticity and regenerative potential in
389 Drosophila by p53. Dev Biol. 2012;361(2):263-76.
390 19. Neufeld TP, de la Cruz AF, Johnston LA, Edgar BA. Coordination of growth and cell division in the
391 Drosophila wing. Cell. 1998;93(7):1183-93.
392 20. Tozluoglu M, Duda M, Kirkland NJ, Barrientos R, Burden JJ, Munoz JJ, et al. Planar Differential
393 Growth Rates Initiate Precise Fold Positions in Complex Epithelia. Dev Cell. 2019;51(3):299-312 e4.
394 21. McComb S, Chan PK, Guinot A, Hartmannsdottir H, Jenni S, Dobay MP, et al. Efficient apoptosis
395 requires feedback amplification of upstream apoptotic signals by effector caspase-3 or -7. Sci Adv.
396 2019;5(7):eaau9433.

397 22. Fujita E, Egashira J, Urase K, Kuida K, Momoi T. Caspase-9 processing by caspase-3 via a feedback
398 amplification loop in vivo. Cell Death Differ. 2001;8(4):335-44.
399 23. Florentin A, Arama E. Caspase levels and execution efficiencies determine the apoptotic
400 potential of the cell. J Cell Biol. 2012;196(4):513-27.
401 24. Verghese S, Su TT. Drosophila Wnt and STAT Define Apoptosis-Resistant Epithelial Cells for
402 Tissue Regeneration after Irradiation. PLoS Biol. 2016;14(9):e1002536.
403 25. Johnston LA, Edgar BA. Wingless and Notch regulate cell-cycle arrest in the developing
404 Drosophila wing. Nature. 1998;394(6688):82-4.
405 26. Bergmann A, Agapite J, McCall K, Steller H. The Drosophila gene hid is a direct molecular target
406 of Ras-dependent survival signaling. Cell. 1998;95(3):331-41.
407 27. Lu Q, Schafer DA, Adler PN. The Drosophila planar polarity gene multiple wing hairs directly
408 regulates the actin cytoskeleton. Development. 2015;142(14):2478-86.
409 28. Brown J, Bush I, Bozon J, Su TT. Cells with loss-of-heterozygosity after exposure to ionizing
410 radiation in Drosophila are culled by p53-dependent and p53-independent mechanisms. PLoS Genet.
411 2020;16(10):e1009056.
412 29. Baker BS, Carpenter AT, Ripoll P. The Utilization during Mitotic Cell Division of Loci Controlling
413 Meiotic Recombination and Disjunction in DROSOPHILA MELANOGASTER. Genetics. 1978;90(3):531-78.
414 30. Zhou L, Schnitzler A, Agapite J, Schwartz LM, Steller H, Nambu JR. Cooperative functions of the
415 reaper and head involution defective genes in the programmed cell death of Drosophila central nervous
416 system midline cells. Proc Natl Acad Sci U S A. 1997;94(10):5131-6.
417 31. Lawrence PA, Sanson B, Vincent JP. Compartments, wingless and engrailed: patterning the
418 ventral epidermis of Drosophila embryos. Development. 1996;122(12):4095-103.
419 32. Verghese S, Bedi S, Kango-Singh M. Hippo signalling controls Dronc activity to regulate organ
420 size in Drosophila. Cell Death Differ. 2012;19(10):1664-76.
421 33. Charan J, Kantharia ND. How to calculate sample size in animal studies? J Pharmacol
422 Pharmacother. 2013;4(4):303-6.
423
424

425 **Figure Legends**
426
427 **Figure 1. Optimizing temperature shift conditions to detect cells with X-ray-induced past caspase**
428 **activity**
429 Larvae were treated as in Fig. 1A where T= 29°, 26°, 22° or 18°C as indicated on the panels. Wing discs
430 were dissected at 72h after exposure to 0R (-IR) or 4000R (+IR), fixed, stained for DNA, and imaged for
431 DNA and GFP. CasTrk = Caspase Tracker. CasEx = CasExpress. The genotype of the wing discs shown was
432 CasExpress/G-trace; GAL80^{ts}/+ in all panels except (I) which shows a control CasExpress mutant with a
433 DQVD>DQVA mutation that renders the GAL4 membrane tether caspase-resistant. Scale bar = 120
434 microns.
435 (A) The experimental protocol
436 (B) Fractional area of each disc that is GFP+ was quantified in Image J. p-values were calculated
437 using a 2-tailed t-test. The numbers in the brackets are the number of discs analyzed in two to four
438 biological replicate experiments per sample.
439 (C-C') An unirradiated disc shows GFP+ cells even after a short (6h) pulse of heat inactivation of
440 GAL80^{ts} at 29°C.
441 (D-D') An irradiated disc shows more GFP+ cells with the same temperature shift as in C.
442 (E-G') Unirradiated discs show few GFP+ cells when the temperature shift for 6h is to 18°C (E),
443 22°C (F) or 26°C (G-G').
444 (H-H') A irradiated discs from larvae shifted to 26°C shows robust GFP signal.
445 (I) Discs from caspase-resistant CasExpress mutant larvae treated exactly as in H.
446 (J) Discs from larvae treated exactly as in (H) but with no temperature shift
447
448
449 **Figure 2. XPAC cells are capable of proliferating**
450 Larvae of the genotype CasExpress/G-trace; GAL80^{ts}/+ were treated as in Fig. 1A where T=26°C. Wing
451 discs were dissected at 24, 48 and 72h after exposure to 4000R, fixed, and stained for DNA. The discs
452 were imaged for GFP (A-C), DNA (A'-C') and RFP (A''-C''). N= number of discs examined in three
453 biological replicates for 24h and 2 biological replicates each for 48 and 72h. The arrow points to a singlet
454 GFP+ cell and the arrowhead points to a doublet of GFP+ cells in panel A. Scale bar = 120 microns.
455
456 **Figure 3. XPAC prevalence in development and the effect of apoptotic signaling**
457 Larvae of the genotype CasExpress/G-trace; GAL80^{ts}/+ were treated as in Fig. 1A where T=26°C. Wing
458 discs were dissected at 24h after exposure to 4000R, fixed, and stained for DNA. Scale bar = 120
459 microns. p-values were calculated using a 2-tailed t-test.
460 (A-D') The discs were imaged for DNA (A-D) or GFP (A'-D'). Hinge folds are visible in DNA images
461 of more developed discs and are indicated with arrowheads in (C-D). n = notum and w = future wing that
462 includes the hinge and the pouch. The most distal region of the future wing is indicated with * in (A'-C');
463 GFP+ cells clear from this region before the rest of the future wing. A ring of GFP+ cells is indicated with
464 arrows (C').
465 (E-E') CasExpress/G-trace; GAL80^{ts}/+ larvae that also carried one copy of UAS-hid, rpr on the X
466 chromosome were treated as in (A-D).
467 (F) The % of disc area that is GFP+ was quantified from discs such as those shown in A'-D' and
468 plotted against the total disc area. The numbers of discs analyzed are in parentheses. The data are from
469 3 (6-7d) and 2 (7-8d) biological replicates each.
470 (G) The % of disc area that is GFP+ was quantified for discs with no epithelial folds (less
471 developed discs such as those in A and B) and discs with epithelial folds (more developed discs such as
472 those in C and D). The data are from 6 biological replicate samples of larvae 7-8d old at irradiation.

473 (H-I) The % of disc area that is GFP+ was quantified from discs such as those shown in E' and
474 plotted against the total disc area. The number of discs analyzed are in parentheses.
475 The genotypes were:
476 Control = CasExpress/G-trace; GAL80^{ts}/+
477 hid, rpr = UAS-hid, UAS-rpr/+ or Y; CasExpress/G-trace; GAL80^{ts}/+
478 rpr = UAS-rpr/+ or Y; CasExpress/G-trace; GAL80^{ts}/+
479 DroncDN = CasExpress/G-trace; GAL80^{ts}/UAS-Dronc^{DN}
480 H99 = CasExpress/G-trace; GAL80^{ts}/H99
481 p35 = CasExpress/G-trace; GAL80^{ts}/UAS-p35
482
483 **Figure 4. Apoptosis and mitosis are widespread throughout the wing disc**
484 The larvae of the genotype CasExpress/G-trace; GAL80^{ts}/+ were treated as in Fig. 1A where T=26°C.
485 Scale bar = 120 microns.
486 (A-C'') Wing discs were fixed and stained with an antibody to phospho-S10 on Histone H3, a
487 mitotic marker. The dashed line marks the pouch. The discs were also stained for DNA and visualized for
488 CasExpress>GFP. The arrows point to the notum and the dashed lines mark the pouch.
489 (D-F''') Wing discs were fixed and stained with an anti-cleaved-Dcp1 antibody to detect cells that
490 activated apoptotic caspases. The discs were also stained for DNA and visualized for CasExpress>GFP.
491 The arrows point to the notum and the * marks the distal pouch.
492 (G-J) Wing discs were stained live with the vital dye Acridine Orange which reports on apoptotic
493 cells. The brackets mark the hinge region that is resistant to IR-induced apoptosis. The arrows point to
494 the notum and the * marks the distal pouch.
495
496 **Figure 5. Developmental signaling pathways regulate XPAC cell prevalence**
497 (A-E') Larvae of the genotypes indicated below were treated as in Fig. 1A where T=26°C. The
498 discs were dissected 24h after exposure to 4000R, fixed and stained with an antibody against Wg (A-
499 D'''). The discs were also stained for DNA and visualized for CasExpress>GFP. Arrows indicate the notum
500 and * indicate the distal pouch. Arrowheads indicate the Wg Inner Ring (white) or the D/V boundary
501 (yellow).
502 (F-G) The GFP+ areas were quantified and expressed as % of the total disc area. p-values were
503 calculated using a 2-tailed t-test. Scale bar = 120 microns. The genotypes were:
504 Control = CasExpress/G-trace; GAL80^{ts}/+
505 wg = CasExpress/G-trace; GAL80^{ts}/UAS-wg
506 Axin = CasExpress/G-trace; GAL80^{ts}/UAS-Axin
507 NotchICD = CasExpress/G-trace; GAL80^{ts}/UAS-N^{ICD}
508 mam-delta = CasExpress/G-trace; GAL80^{ts}/UAS-mam$^{\Delta}$
509 RasV12 = CasExpress/G-trace; GAL80^{ts}/UAS-Ras^{V12}
510
511 **Figure 6. Cells with past caspase activity show reduced IR-induced LOH**
512 (A-F) Adult wings from larvae of the genotype CasExpress/G-trace; GAL80^{ts}/mwh^{1}. The
513 experimental protocol shown in Fig. 1A was followed but larvae were aged for 6d at 18°C after egg
514 collection to get 6-7d old larvae (A-C) or aged for 7d at 18°C after egg collection to get 7-8d old larvae at
515 the time of irradiation. Larvae were irradiated with 0 or 4000R of X-rays. After incubation at 26°C, larvae
516 were returned to 18°C for the remainder of the experiment. The two +IR wings shown for each group
517 represent the range of clone size and number observed in two biological replicate experiments. The
518 number of wings examined was 12 (6-7d -IR) , 9 (6-7d +IR). 6 (7-8d -IR) and 11 (7-8d +IR), in two
519 biological replicate experiments each.

520 (G) A region of the wing was imaged at 4X magnification relative to A-F. It is possible to discern
521 the top (in focus, arrow) and the bottom (out-of-focus, arrowhead) surfaces of the wing in such images.
522 (H) A region of the wing is shown magnified 16X relative to A-F. It is possible to assign mwh state
523 to individual GFP+ cells, for example, 3 cells within dashed lines. In a patch of mwh cells (white line),
524 none are GFP+.
525 (I) Percent of image area that is mwh was quantified from images such as G, for the GFP+ and
526 GFP- portion of the surface in focus. The data include wings from animals irradiated as 6-7d (gray) or 7-
527 8d (black) old larvae. Each dataset also shows a significant difference in mwh between GFP- and GFP+
528 areas: p= 0.04 for 6-7d and 0.03 for 7-8d. p-values were computed using a 2-tailed t-test.
529 (J-K'''') Larvae of the genotype CasExpress/G-trace; GAL80^{ts}/+ were treated as in Fig. 1A. Wing
530 discs were dissected at 20-22h after irradiation with 4000R, fixed and stained with an antibody against γ-
531 H2Av. The discs were also stained for DNA and imaged for GFP. Arrowheads in J'''' indicate rare cells in
532 which GFP and γ-H2Av signals overlap to appear white. The boxed area in J''' is magnified in K-K''''. L-L'''
533 show a magnified area of another disc, to demonstrate reproducibility. A total of 52 discs were
534 examined in 3 biological replicate experiments.
535 Scale bar = 960 microns in A-F, 120 microns in J and 48 microns in K-L.
536
537 **S1 Figure. Caspase cleavage without IR and DNA double strand breaks with and without IR.**
538 Larvae of the genotype CasExpress/G-trace; GAL80ts/+ were treated as in Fig. 1A where T=26°C. Wing
539 discs were dissected at 4h after exposure to 0 or 4000R of X-rays, fixed, and stained for DNA and with
540 antibodies to cleaved Dcp1 (A-A') or γ-H2Av (B-C'). The scale bar = 120 microns in A and 24 microns in B-
541 C.
542
543 **S1 Table. Fly stocks used.**

FIGURE 1

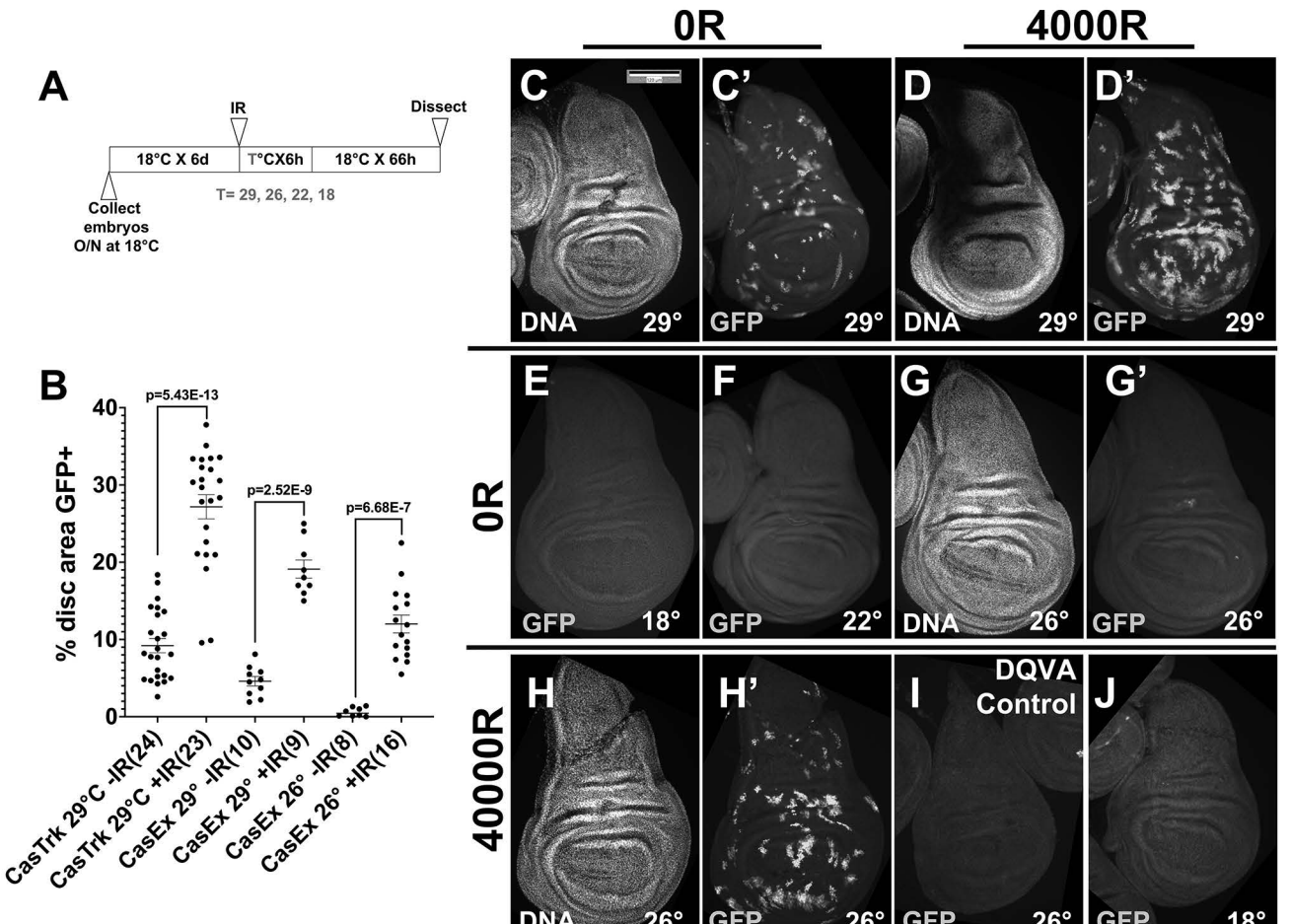
A
IR
Dissect
18°C X 6d
T°CX6h
18°C X 66h
T= 29, 26, 22, 18
Collect embryos O/N at 18°C
B
% disc area GFP+
p=5.43E-13
p=2.52E-9
p=6.68E-7
CasTrk 29°C -IR(24)
CasTrk 29°C +IR(23)
CasEx 29° -IR(10)
CasEx 29° +IR(9)
CasEx 26° -IR(8)
CasEx 26° +IR(16)
0R
4000R
C
C'
D
D'
DNA 29°
GFP 29°
DNA 29°
GFP 29°
0R
E
F
G
G'
GFP 18°
GFP 22°
DNA 26°
GFP 26°
40000R
H
H'
I
J
DQVA Control
DNA 26°
GFP 26°
GFP 26°
GFP 18°

FIGURE 2

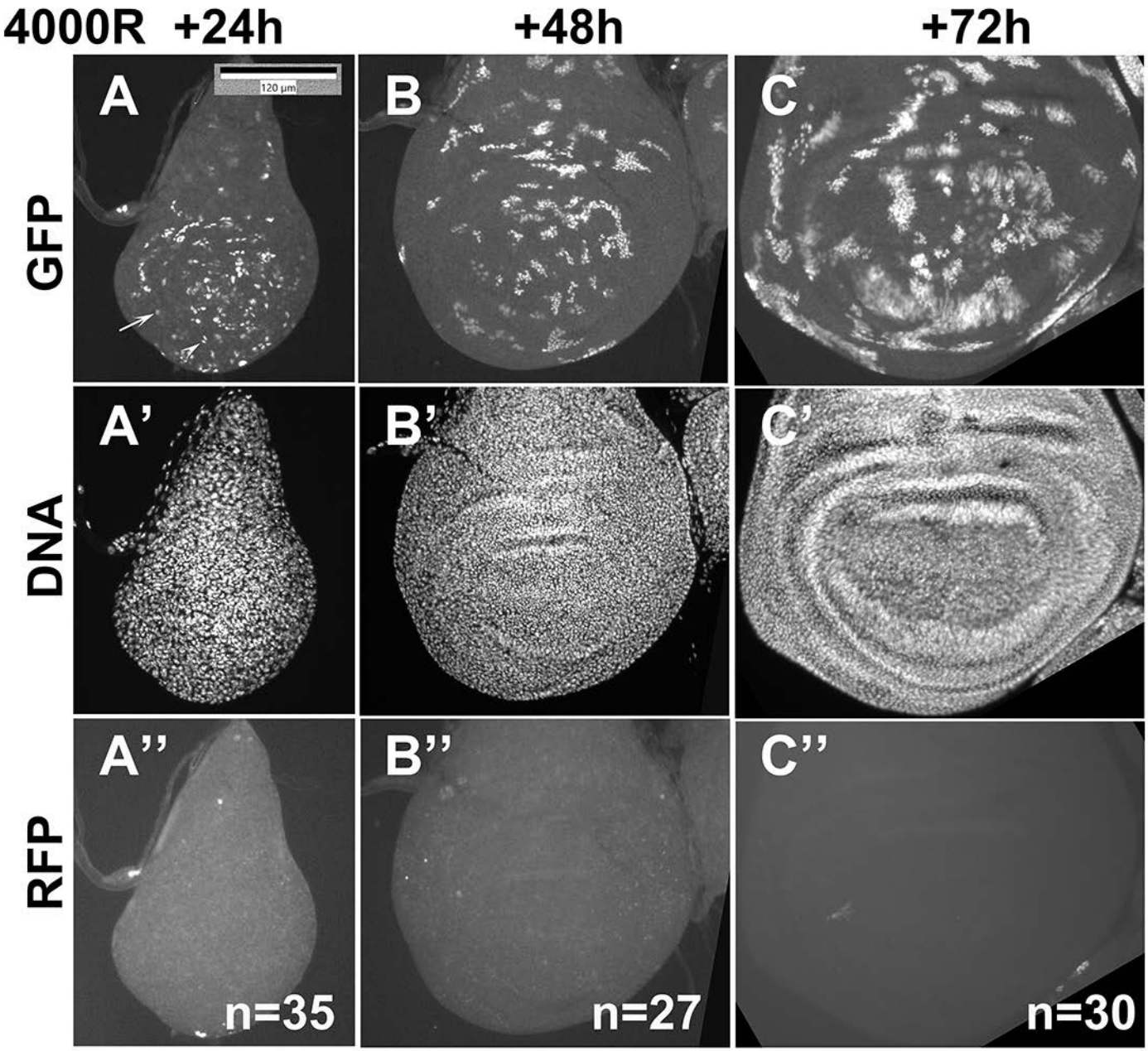

FIGURE 3

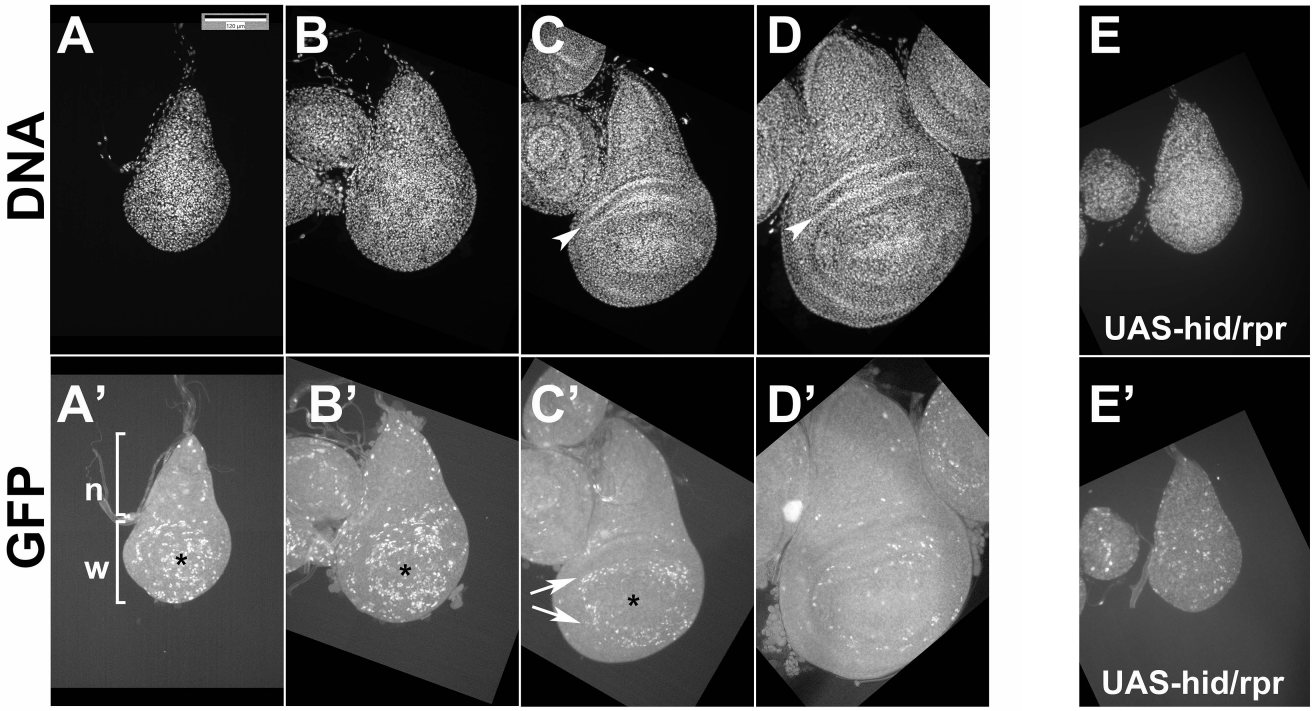
DNA
GFP
A
B
C
D
E
A'
B'
C'
D'
E'
n
w
*
UAS-hid/rpr
UAS-hid/rpr

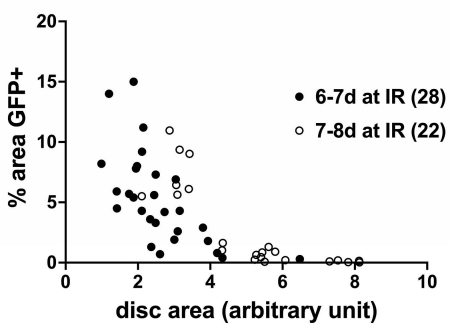
F
% area GFP+
disc area (arbitrary unit)
6-7d at IR (28)
7-8d at IR (22)
0
5
10
15
20
0
2
4
6
8
10

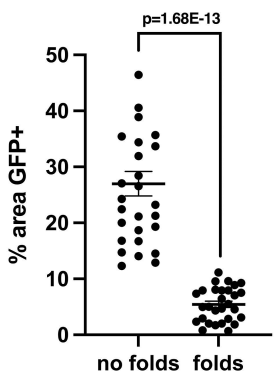
G
p=1.68E-13
% area GFP+
no folds
folds
0
10
20
30
40
50

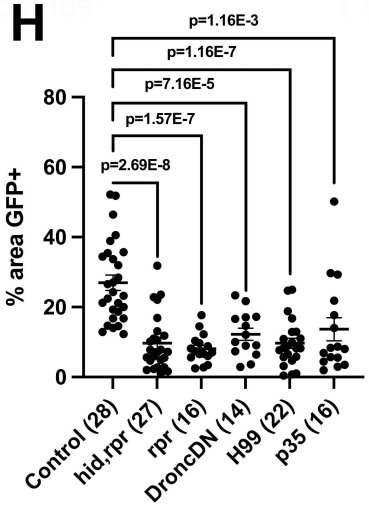
H
p=1.16E-3
p=1.16E-7
p=7.16E-5
p=1.57E-7
p=2.69E-8
% area GFP+
0
20
40
60
80
Control (28)
hid,rpr (27)
rpr (16)
DroncDN (14)
H99 (22)
p35 (16)

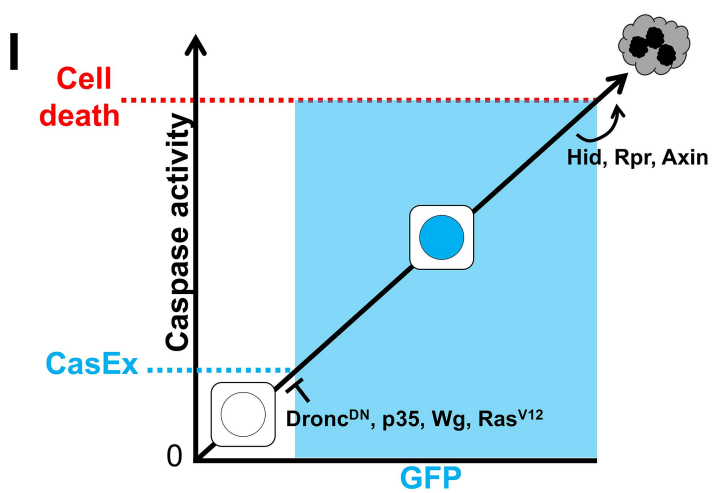
I
Cell death
CasEx
Caspase activity
0
GFP
Hid, Rpr, Axin
Dronc^{DN}, p35, Wg, Ras^{V12}

FIGURE 4

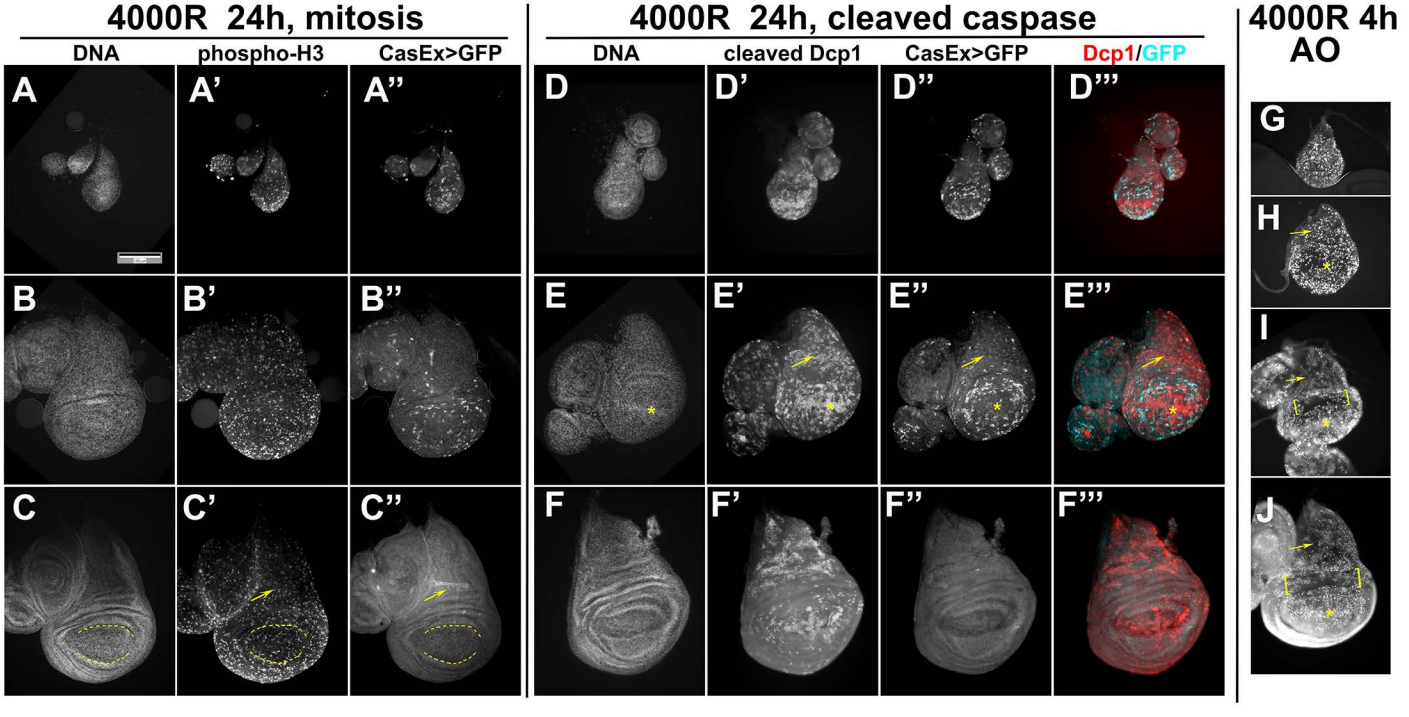
4000R 24h, mitosis
DNA
phospho-H3
CasEx>GFP
A
A'
A''
B
B'
B''
C
C'
C''
4000R 24h, cleaved caspase
DNA
cleaved Dcp1
CasEx>GFP
Dcp1/GFP
D
D'
D''
D'''
E
E'
E''
E'''
F
F'
F''
F'''
4000R 4h AO
G
H
I
J

FIGURE 5

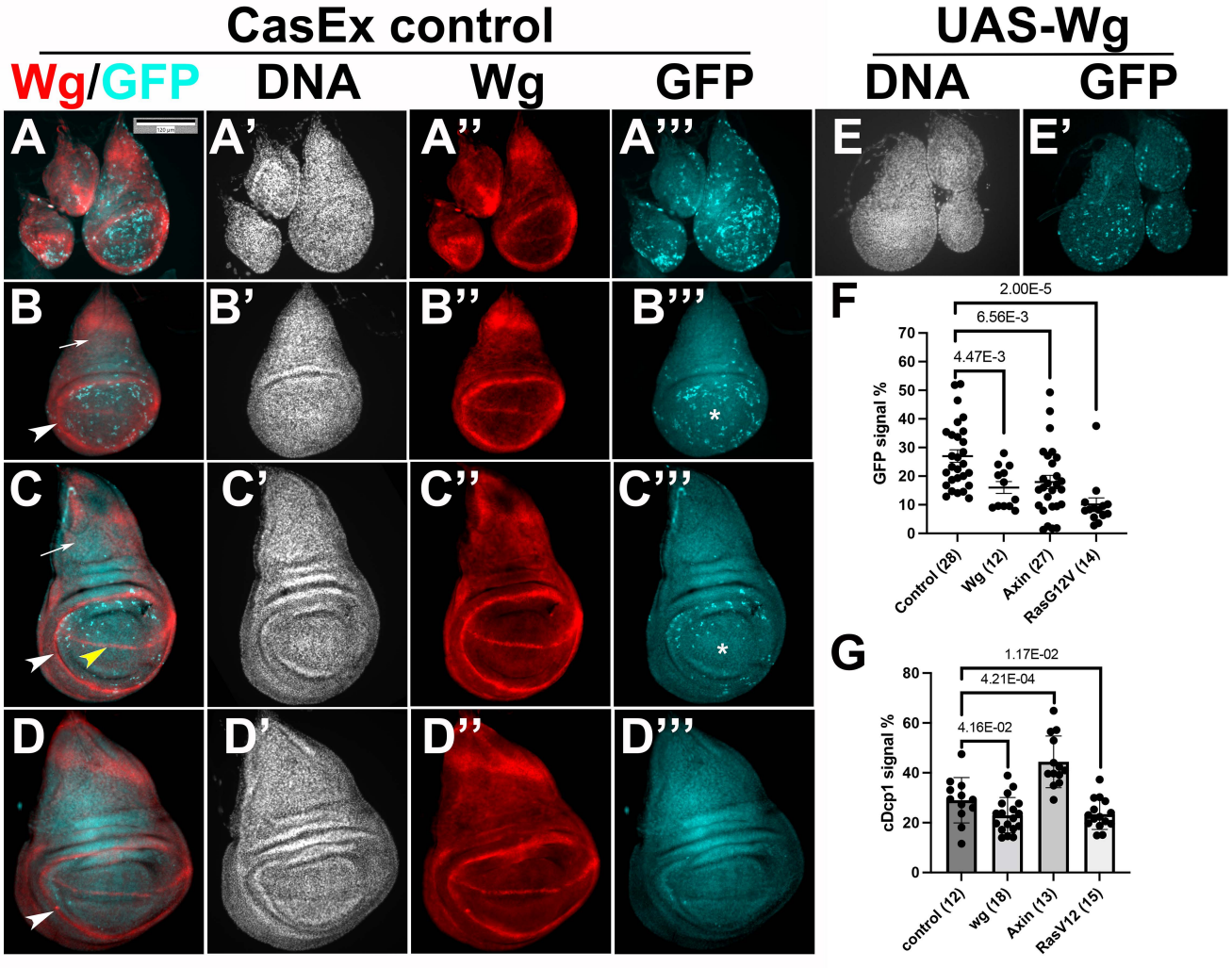
CasEx control
UAS-Wg
Wg/GFP
DNA
Wg
GFP
DNA
GFP
A
A'
A''
A'''
E
E'
B
B'
B''
B'''
C
C'
C''
C'''
D
D'
D''
D'''
F
2.00E-5
6.56E-3
4.47E-3
GFP signal %
Control (28)
Wg (12)
Axin (27)
RasG12V (14)
G
1.17E-02
4.21E-04
4.16E-02
cDcp1 signal %
control (12)
wg (18)
Axin (13)
RasV12 (15)

FIGURE 6

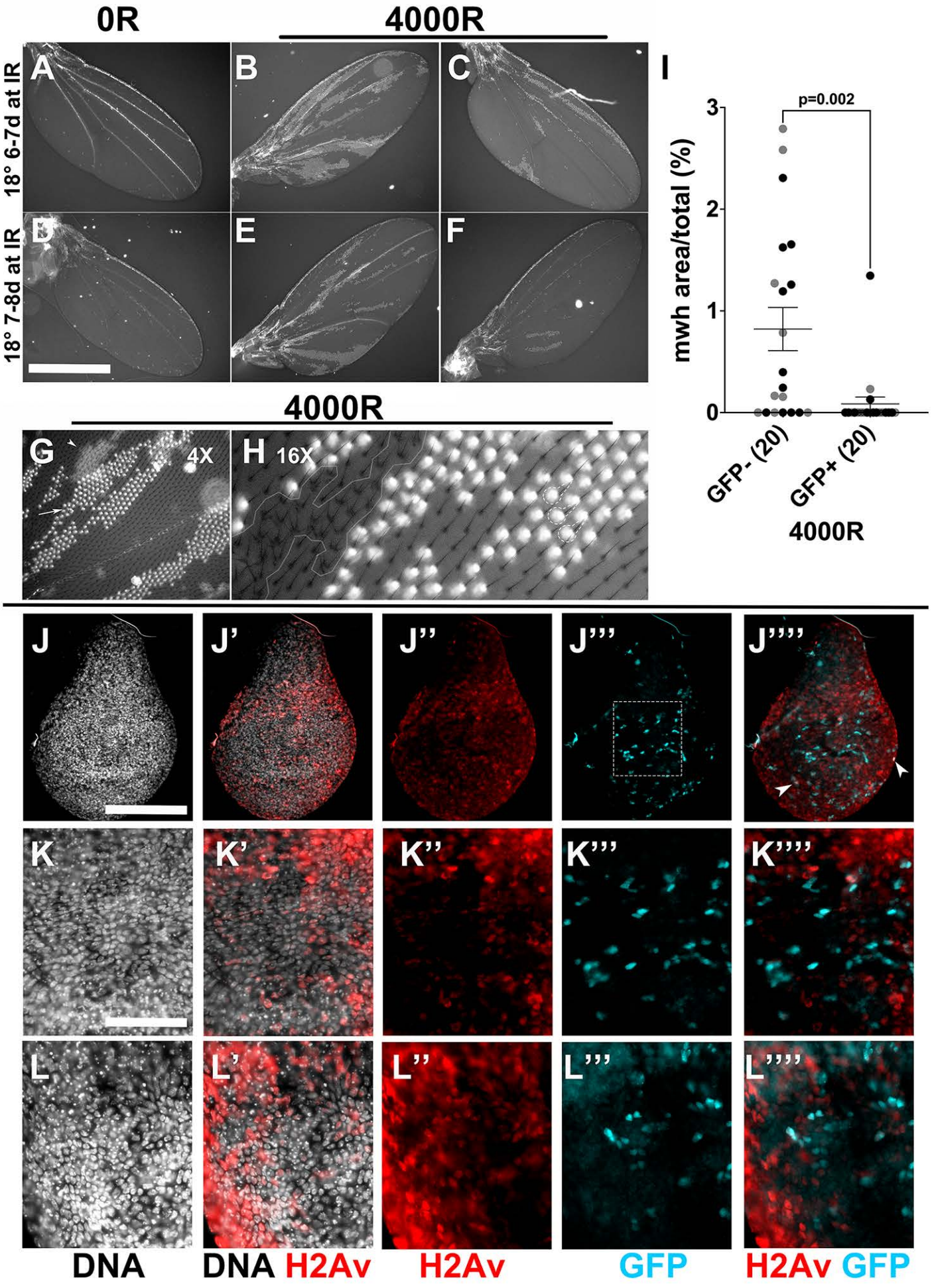
0R
4000R
18° 6-7d at IR
18° 7-8d at IR
A
B
C
D
E
F
I
p=0.002
mwh area/total (%)
3
2
1
0
GFP- (20)
GFP+ (20)
4000R
4000R
G
4X
H
16X
J
J'
J''
J'''
J''''
K
K'
K''
K'''
K''''
L
L'
L''
L'''
L''''
DNA
DNA H2Av
H2Av
GFP
H2Av GFP

S1 Figure

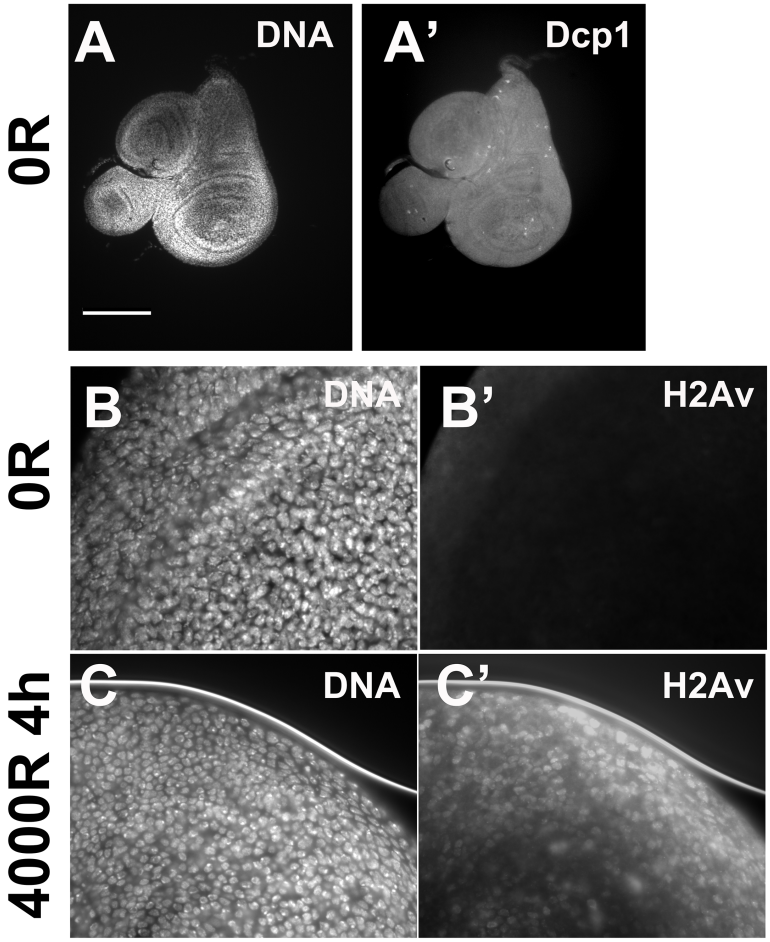

S1 Figure. Caspase cleavage without IR and DNA double strand breaks with and without IR.
Larvae of the genotype CasExpress/G-trace; GAL80ts/+ were treated as in Fig. 1A where T=26°C. Wing discs were dissected at 4h after exposure to 0 or 4000R of X-rays, fixed, and stained for DNA and with antibodies to cleaved Dcp1 (A-A') or γ-H2Av (B-C'). The scale bar = 120 microns in A and 24 microns in B-C.

S1 Table. Fly stocks used

Source (BL = Bloomington Stock Center)	Used in Fig.	Genotype
BL28280 'G-trace'	all	P{w[+mC]=UAS-RedStinger}4, P{w[+mC]=UAS-FLP.D}JD1, P{w[+mC]=Ubi-p63E(FRT.STOP)Stinger}9F6
BL65419	all	P{w[+mC]=Ubi-CasExpress}attP40
BL7017	all	tub-GAL80^{ts} on chromosome III
BL65420	1	P{w[+mC]=Ubi-CasExpress.DQVA}attP40
Ref 12	1	Caspase Tracker
BL1576	3	Do(3L)H99/TM6B Tb
BL5823	3	w1118 P{UAS-rpr.C}27 (UAS-rpr on the X chromosome)
Ref 30	3	UAS-hid, UAS-rpr on the X chromosome
BL5073	3	w[*]; P{w[+mC]=UAS-p35.H}BH2
Ref 32	3	UAS-Dronc^{DN} on chromosome III
Ref 31	5	UAS-Wg on chromosome III
BL7225	5	w[*]; Kr[If-1]/CyO; P{w[+mC]=UAS-Axn.GFP}3 (UAS-Axin on chromosome III)
BL64195	5	w[*]; P{w[+mC]=UAS-Ras85D.V12}TL1 (constitutively active Ras on Ch. III)
BL549	6	mwh[1]